RSC Advances

PAPER

View Article Online
View Journal | View Issue



Cite this: *RSC Adv.*, 2021, **11**, 29986

# ATRP-based synthesis of a pH-sensitive amphiphilic block polymer and its self-assembled micelles with hollow mesoporous silica as DOX carriers for controlled drug release

Xiuxiu Qi,†* Hongmei Yan † and Yingxue Li

Received 19th May 2021
Accepted 3rd August 2021

DOI: 10.1039/d1ra03899k

rsc.li/rsc-advances

The atom transfer radical polymerization (ATRP)-based synthesis of a pH-sensitive fluorescent polymer (PSDMA-*b*-POEGMA) was successfully prepared using 3,6-dibromo-isobutyramide acridine (DIA), an initiator with a fluorescent chromophore, to initiate a lipophilic monomer 2-styryl-1,3-dioxan-5-yl methacrylate (SDMA) and a hydrophilic monomer oligo(ethylene glycol) methyl ether (OEGMA), which contained a cinnamic aldehyde acetal structure. With the addition of hollow mesoporous silicon (HMS@C18), the pH-sensitive core–shell nanoparticles (HMS@C18@PSDMA-*b*-POEGMA) were developed *via* a self-assembly process as carriers for the anticancer drug doxorubicin (DOX) for drug loading and controlled release. The nanocomposites showed a higher drug loading capacity which was much higher than that observed using common micelles. At the same time, the polymer coated on the surface of the nanoparticles contains the fluorescent segment of an initiator, which can be used for fluorescence contrast of the cells. The nanocomposite carrier selectively inhibits human melanoma cell A375 relative to human normal fibroblasts GM. The *in vitro* results suggested that a smart pH sensitive nanoparticles drug delivery system was successfully prepared for potential applications in cancer diagnosis and therapy.



## 1 Introduction

In recent years, polymeric drug carriers have become a hot topic in the study of controlled release systems. A drug carrier is a system that can change the way in which drugs enter and are distributed within the body, control the rate of release of drugs and deliver drugs to targeted organs. As various drug delivery and targeting systems can reduce drug degradation and loss, reduce side effects, and improve bioavailability, research in these areas has attracted increased attention.

As one of the most important synthetic methods of polymers, free radical polymerization can be used to prepare amphiphilic random copolymers. Lu's group performed the conventional free radical copolymerization of methacrylate containing a cyclic acetal structure and 2-hydroxyethyl acrylate under the initiation of azobisisobutyronitrile and obtained an amphiphilic copolymer that could encapsulate small molecules of drugs and could control the release of drugs in a weakly acidic environment.[1] On the other hand, owing to its own limitations, such as the existence of chain transfer and chain termination and other side reactions, free radical polymerization cannot accurately control the molecular weight and molecular structure. Since atom transfer radical polymerization (ATRP) was first reported by Matyjaszewski *et al.*[2,3] in 1995, the ATRP method has increasingly been developed into an effective means to accurately control the structure of polymers, especially for the synthesis of structurally controllable amphiphilic polymers.[4–9]

Compared with polymer micelles, large pore mesoporous silica (LPMSN) and hollow mesoporous silica nanoparticles (HMS) can significantly improve drug loading, and the silicon spheres have a good biocompatibility, good monodispersibility and slow-release ability, therefore they have attracted extensive attention in the field of biomedical materials. However, unmodified LPMSN and HMS nanoparticles cannot achieve "zero release" and controlled release before reaching the lesion site. In order to possess a wide range of clinical applications, they must be modified to enable controlled release.[10–16] As the pH-controlled release mechanism can be adapted to the special physiological environment of the tumor site, the modification of pH-sensitive polymers on the surface of HMS is a very promising method for the preparation of controlled release drug carriers. Lu's group has reported a series of experiments in this regard.[17–19]

In this paper, the fluorescent amphiphilic block copolymer (PSDMA-*b*-POEGMA) containing a cinnamic aldehyde acetal structure was synthesized by ATRP using the initiator 3,6-dibromo-isobutyramide acridine (DIA) with a fluorescent

*Changzhou Vocational Institute of Engineering, 33 Gehu Road, Changzhou, Jiangsu, China. E-mail: xiuxiu_qi01@sina.com; Fax: +86 519 86332160; Tel: +86 519 86332160*

† Xiuxiu Qi and Hongmei Yan contributed equally to this work.

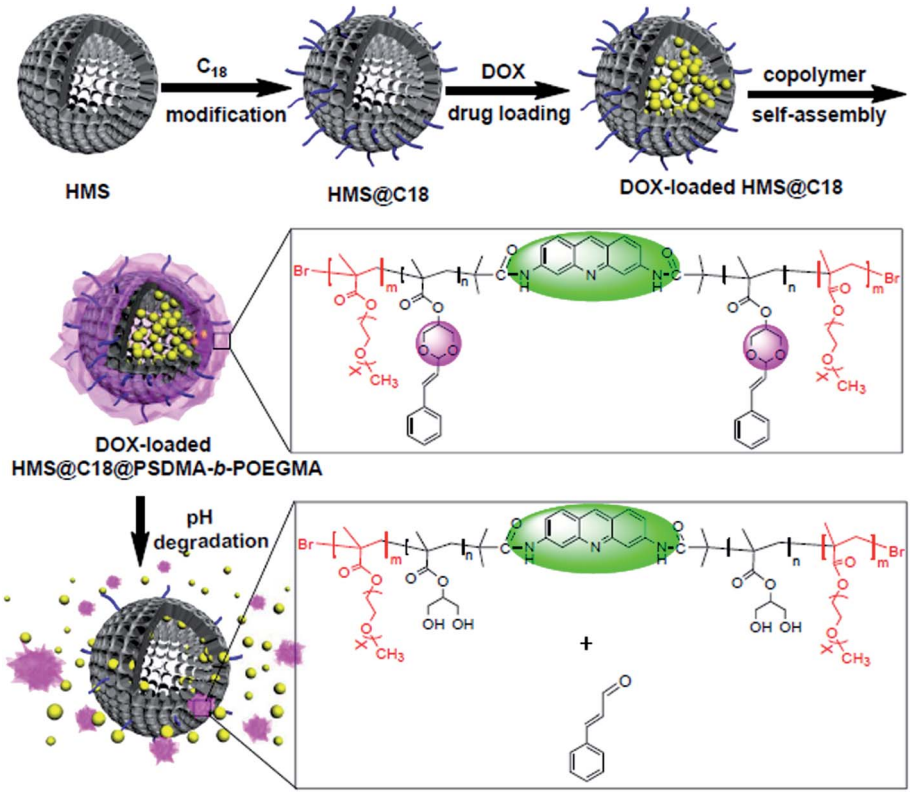


Scheme 1 Schematic diagram of the synthesis of the pH-sensitive amphiphilic block copolymer and self-assembly with C18-modified HMS.

chromophore. The wrapping of the HMS resulted in the core–shell nanocomposite system, wherein the system not only has the characteristics of a high drug loading performance and pH-sensitive drug release but can also utilize a fluorescent group to carry out cell imaging, and can selectively inhibit tumor cells as the small molecules of cinnamic aldehyde can be released into the acidic environment of the tumor cells. According to previous work reported by Truong's group,[20] we believe these nanoparticles (HMS@C18@PSDMA-*b*-POEGMA) would be suitable candidates for cancer drug delivery owing to their minimal interactions with immune cells in blood when injected into the body for cancer treatment. The synthesis and self-assembly process of the composite nanoparticles for use as drug carriers is described in Scheme 1.

# 2 Experimental

## 2.1 Raw materials and reagents

Zinc chloride, glycerol, *m*-phenylenediamine, bromoisobutyryl bromide, oxalic acid dihydrate, pentamethyldiethylenetriamine (PMDETA), acryloyloxyethyl trimethyl ammonium chloride 80% aqueous solution (AETAC), and 2,2-azobis(2-methylpropyl imidazole)dihydrochloride (V-50) were purchased from National Pharmaceutical Group Chemical Reagent Co., Ltd. Methyl methacrylate (98%, MMA) was washed with sodium hydroxide solution (5%) and deionized water, dried over anhydrous sodium sulfate, and stored at a low temperature after distillation under reduced pressure. *N*,*N*-Dimethylacrylamide (98%, DMAA) was treated with calcium hydride and distilled under reduced pressure and stored at a low temperature for future use. Cuprous bromide (98.5%, CuBr) was purified by washing with methanol and acetic acid. Oligo(ethylene glycol) methyl ether methacrylate (OEGMA) (average MW ~ 950) was purchased from Alfa Aesar. All other reagents used were analytically pure unless otherwise specified.

## 2.2 Test method and characterization

The $^1$H-NMR analysis was performed using an INOVA 400 MHz NMR instrument (Varian, USA), using $CDCl_3$ and DMSO-$d_6$ as solvents respectively. The results of the elemental analysis were determined using a Carlo Erba-MOD1106 Elemental Analyzer (Kalopa, Italy). Time-of-flight mass spectrometry (TOF-MS) was performed on a Micromas analyzer (UK). The conversion of the monomer reaction was determined by weighing, and the molecular weight and molecular weight distribution were determined using a Waters-1515 gel chromatograph (Waters, USA, column temperature 30 °C) with a mobile phase of *N*,*N*-dimethyl-formamide or tetrahydrofuran. The UV-Vis spectrum was determined using a λ-17 UV-Vis spectrophotometer (PerkinElmer, USA). The fluorescence spectrum was determined using an Edinburgh-920 fluorescence spectrometer (Edinburgh, UK). Dynamic light scattering (DLS) was performed at a test temperature of 25 °C, using a 633 nm He–Ne laser detector. Transmission electron microscopy (TEM) was performed using a TecnaiG220 Type with an acceleration voltage of 200 kV.

### 2.3 Synthesis of the fluorescent initiator DIA

The reaction equation is shown in Scheme 2.[21] Glycerol (10 g) and zinc chloride (5 g) were dissolved with stirring at 120 °C, then 3.5 g of oxalic acid and 3 g of *m*-phenylenediamine were added and the mixture was warmed to 155 °C. After 45 min a viscous liquid was obtained, which was added to 80 mL of 2.5 mol $L^{-1}$ sodium hydroxide. The precipitate was removed by filtration dissolved in as little as 1 M hydrochloric acid, and an excess amount of ammonia was added to remove the excess zinc ions. Glacial acetic acid was used to dissolve the precipitate, and a small amount of 20% sulfuric acid solution was added for treatment. Then the precipitate was crystallized at a low temperature to obtain dark red 3,6-diaminoacridine sulfate. The crude product was subsequently treated with an excess of ammonia, dried at 120 °C and recrystallized from ethanol to give the yellow needle-like crystal product.

$C_{13}H_{11}N_3$ element analysis theoretical value: C, 74.64%, H, 5.26%, N, 20.10%.

Measured value: C, 74.18%, H, 5.29%, N, 20.53%.

$^1$H NMR (400 MHz, acetone-$d_6$), $\delta$ (ppm): 8.35 (s, 1H), 7.64 (d, $J$ = 8.80 Hz, 2H), 6.85 (d, $J$ = 8.77 Hz, 2H), 6.74 (s, 2H), 6.00 (s, 4H).

500 mg of 3,6-diaminoacridine was dissolved in triethylamine solution under nitrogen protection, and 5 mL of bromoisobutyryl bromide was then slowly added dropwise to an ice bath. Immediately after the addition, the ice bath was removed and stirred overnight at room temperature. The product was washed with ether and saturated sodium bicarbonate and the resulting solid was dissolved in as little as possible of *N*,*N*-dimethylformamide and added dropwise to deionized water to precipitate. The brown powder product was obtained after filtration and was dried under vacuum overnight.

$^1$H NMR ($CDCl_3$, 400 MHz), $\delta$ (ppm): 8.78 (s, 2H), 8.63; (s, 1H), 8.29 (s, 2H), 7.95 (d, J = 9.03 Hz, 2H), 7.80 (d, J = 8.81 Hz, 2H), 2.11 (s, 1H).

### 2.4 Synthesis of the pH sensitive monomer 2-styryl-1,3-dioxan-5-yl methacrylate (SDMA)

The synthesis of SDMA was performed according to the method shown in Scheme 3.

**2.4.1 Synthesis of the intermediate (*E*)-2-styryl-1,3-dioxan-5-ol (SDOO).** (*E*)-2-Styryl-1,3-dioxan-5-ol (SDOO) was synthesized according to the previously reported method.[22] To a mixture of 132 g of cinnamic aldehyde and 92 g of glycerol, 5 drops of 40% sulfuric acid solution were added dropwise and stirred, the reaction system was evacuated, and the mixture was slowly heated to 100 °C. The reaction was continued for 30 min until no water was distilled off. It was cooled to room temperature and the reactants gradually solidified. The solid was washed with warm water at 30 °C to remove the unreacted starting material, followed by suction filtration. After this, the solid was dissolved with heated benzene, the liquid was separated, the benzene phase was dried over anhydrous magnesium sulfate, filtered while hot, cooled to room temperature, and a pale yellow solid was precipitated, followed by suction filtration, and the solid was then dried and recrystallized from benzene to obtain 38 g of asbestos-like needle crystals. The yield was 18% and the melting point was 121 °C.

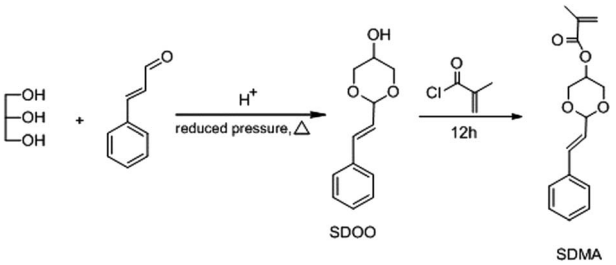


Scheme 3 Outline schematic diagram for the synthesis of SDMA.

$^1$H NMR (400 MHz, DMSO-$d_6$, $\delta$, ppm): 3.46 (s, 1H), 3.90 (dd, 4H), 4.90 (d, 1H), 5.16 (m, 1H), 6.20 (q, 1H), 6.70 (d, 1H), 7.28 (t, 1H), 7.35 (t, 2H), 7.46 (d, 2H).

Elem. Anal. Calcd for $C_{12}H_{14}O_3$: C, 69.88; H, 6.84. Found: C, 69.38; H, 6.687.

TOF-MS (EI): calcd for $C_{12}H_{14}O_3$: 206.0943, found: 206.0941.

**2.4.2 Synthesis of the monomer SDMA.** SDOO 27.4 g (0.1 mol) was dissolved in 100 mL THF and 10.1 g (0.1 mol) of triethylamine in an ice bath, 10.45 g (0.1 mol) of methacryloyl chloride was added dropwise, and the resulting solution was mixed at room temperature overnight.

The resulting solution was filtered, evaporated to dryness, and recrystallized in ethanol to obtain white crystals. The yield was 45%.

$^1$H NMR (400 MHz, DMSO-$d_6$, $\delta$, ppm): 1.92 (s, 3H), 4.08 (d, 4H), 4.67 (d, 1H), 5.27 (s, 1H), 5.74 (s, 1H), 6.11 (s, 1H), 6.21 (dd, 1H), 6.72 (d, 1H), 7.28 (t, 1H), 7.35 (t, 2H), 7.48 (d, 2H).

Elem. Anal. Calcd for $C_{16}H_{18}O_4$: C, 70.06; H, 6.61. Found: C, 70.06; H, 6.673.

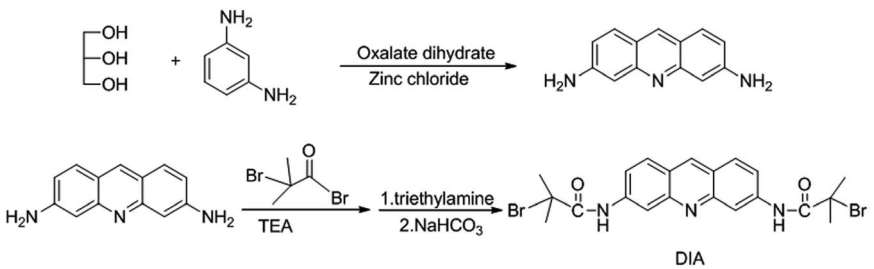


Scheme 2 Synthetic route for the initiator DIA.

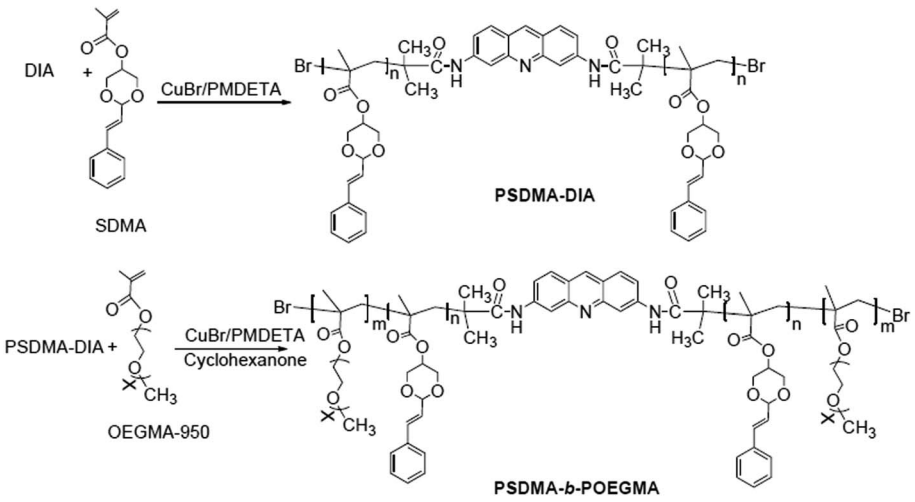


Scheme 4 Synthesis of PSDMA-*b*-POEGMA.

TOF-MS (EI): calcd for $C_{16}H_{18}O_4$: 274.1205, found: 274.1206.

### 2.5 Synthesis of the macromolecular initiator (PSDMA-DIA)

The synthesis of SDMA was performed according to Scheme 4.

DIA (25.3 mg, 0.05 mmol) and 2.74 g (10 mmol) of SDMA were placed in a 25 mL round-bottomed flask, 42 μ L (0.2 mmol) of PMDETA was added, 14.4 mg (0.1 mmol) of CuBr was weighed and added rapidly, and 5 mL of cyclohexanone was also placed in the vessel, the flask was cyclically evacuated and charged with nitrogen three times, and placed in an oil bath at 70 °C to react for 6 h. After completion of the reaction, excess Cu ions were removed by passing through a neutral alumina column, evaporated to dryness, dissolved in as little DMF as possible and precipitated in ether, before being centrifuged to give a yellowish-brown viscous oil which was dried under vacuum overnight. The resulting product was PSDMA-DIA.

$^1$H NMR (400 MHz, DMSO-$d_6$, $\delta$, ppm): 0.6–1.0 (–C**H$_3$**); 1.6–2.0 (–C**H$_2$**–C(CH$_3$)–COO–); 4.3–4.7 (–(C**H$_2$**O)$_2$CH–); 5.1–5.3 (–C**H**(CH$_2$O–)$_2$–); 6.2–6.3 (=C**H**CH(OCH$_2$)$_2$); 6.7–6.8 (=C**H**–C$_6$H$_5$); 7.2–7.6(–C$_6$**H$_5$**).

### 2.6 Synthesis of the amphiphilic block polymer (PSDMA-*b*-POEGMA)

1.37 mg (0.1 mmol) of PSDMA-DIA and 19 g (20 mmol) of OE GMA-950 were placed in a 25 mL round-bottomed flask, 42 μ L (0.2 mmol) of PMDETA, 14.4 mg (0.1 mmol) of rapidly weighed CuBr, and 5 mL of cyclohexanone were added, the flask was cyclically evacuated and charged with nitrogen three times, and then reacted overnight in an oil bath at 70 °C. After the reaction, excess Cu ions were removed by passing through a column of neutral alumina, the eluent was evaporated *in vacuo*, dissolved in as little DMF as possible and precipitated in ether, and centrifuged to give a pale yellow solid, which was dried under vacuum overnight. The resulting product was PSDMA-*b*-POEGMA. The reaction time can be changed to obtain three block copolymers.

$^1$H NMR (4500 MHz, DMSO-$d_6$, $\delta$, ppm): 0.6–1.0 (–C**H$_3$**); 1.6–2.0 (–C**H$_2$**–C(CH$_3$)–COO–); 3.2–3.4 (C**H$_3$**–O–); 3.4–3.6 (–C**H$_2$**(-OCH$_2$CH$_2$–)$_2$–); 4.3–4.7 (–(C**H$_2$**O)$_2$CH–); 5.1–5.3 (–C**H**(CH$_2$O–)$_2$–); 6.2–6.3 (=C**H**CH(OCH$_2$)$_2$); 6.7–6.8 (=C**H**–C$_6$H$_5$); 7.2–7.6 (–C$_6$**H$_5$**).

$^{13}$C NMR (75 MHz, DMSO-$d_6$, $\delta$, ppm): 176.2, 136.7, 134.2, 128.8–128.2, 125.9, 108.4, 80.2, 71.9, 70.7–69.7, 67.8, 62.1, 59.8, 36.9, 25.8.

The gel permeation chromatography (GPC) results for PSDMA-*b*-POEGMA are presented in Table 1.

### 2.7 Preparation of HMS and its self-assembly with polymers

**2.7.1 Synthesis of the polystyrene (PS) template.** In a 500 mL round-bottomed flask, 1.0 g of AETAC was dissolved in 390.0 g of water and 40 g of styrene was added dropwise with mechanical stirring (800 rpm). The resulting mixture was purged with nitrogen for 15 min and heated to 90 °C in an oil bath. 10 mL of an aqueous solution containing 1.0 g of V-50 was added to the above described mixture, and the mixture was stirred at 90 °C for a further 24 h. The resulting white emulsion was centrifuged (16 000 rpm, 15 min) to obtain a white solid, which was washed several times with anhydrous ethanol and dried *in vacuo* to obtain 0.93 g of white powder, this is the PS template.

Table 1 GPC data for the polymers

| Run | Sample name | Conversion (%) | Mw | Mn | Polydispersity index |
|---|---|---|---|---|---|
| 1 | PSDMA$_{50}$-DIA | 95 | 18 200 | 13 700 | 1.33 |
| 2 | PSDMA$_{50}$-*b*-POEGMA$_{72}$ | 91 | 118 200 | 82 100 | 1.44 |
| 3 | PSDMA$_{50}$-*b*-POEGMA$_{56}$ | 93 | 96 300 | 66 900 | 1.43 |
| 4 | PSDMA$_{50}$-*b*-POEGMA$_{42}$ | 90 | 73 400 | 53 600 | 1.37 |

**2.7.2 Synthesis of HMS.** 0.8 g of cetrimonium bromide (CTAB) was dissolved in a mixed solution containing 29.0 g of water, 12.0 g of ethanol and 1.0 mL of ammonia, and the resulting 0.93 g of the PS template was ultrasonically dispersed in 10.0 g of water and added to the above solution of CTAB and stirred for 1 h. After stirring, 4.0 g of the silicon source TEOS was added dropwise, and the stirring was continued for 48 h. After that, the samples were centrifuged (7500 rpm, 15 min), the obtained white solid was washed with water and ethanol several times, and dried under vacuum. The obtained white powder was calcined at 600 °C for 8 h to obtain HMS.

**2.7.3 Modification of HMS (HMS@C18).** After ultrasonic dispersion of 100 mg HMS in 20 mL of anhydrous acetonitrile 5 mg of C18 was added. After stirring for 24 h, the mixture was collected by centrifugation, washed multiple times with a large amount of acetonitrile and ethanol, and dried under vacuum to obtain the product HMS@\C18.

**2.7.4 Self-assembly of HMS@C18 and PSDMA-*b*-POEGMA.** 20 mg of HMS@C18 and SDMA-*b*-OEGMA-DIA with the same mass were respectively taken and added into 1 mL tetrahydrofuran, once they had dissolved 2 mL of deionized water was added dropwise, and the solution was stirred for 24 h. After volatilization of the tetrahydrofuran during the process of micelle formation of the amphiphilic polymer, the hydrophobic HMS@C18 is coated inside, forming the core–shell composite nanoparticles HMS@C18@PSDMA-*b*-POEGMA.[23] The PSDMA-*b*-POEGMA with different compositions were assembled with HMS@C18, and the most suitable polymer for coating was determined to be PSDMA50-*b*-POEGMA72 through the self-assembly effect, as shown in the TEM photos, therefore the following experiments were conducted using this polymer.

## 2.8 Drug loading and release

To test the drug carrier loading and release properties of HMS@C18@PSDMA-*b*-POEGMA, the drug doxorubicin (DOX) was evaluated as a dummy drug. Doxorubicin is obtained by desalting its hydrochloride salt, 1 mg of doxorubicin hydrochloride (DOX-HCl) was added to 187.5 μL of dimethyl sulfoxide (DMSO) and immediately dissolved to give an orange-red solution. Then, 0.48 mL triethylamine was added, and the system changed from orange to deep violet red, the solution was stirred overnight. The system was delaminated and as much as possible of the upper colorless liquid was carefully sucked away. The volume of the lower purplish red solution was about 187.5 μL, and the concentration of DOX at this time was 5 mg $mL^{-1}$. Then, 8, 4 and 0.8 mg of the composite nanocarrier were added into three serum vials, and 5 mL of ultra-pure water was added into each vial, followed by shaking and centrifugation. The remaining solutions were subjected to a DOX concentration test using a fluorescence spectrometer ($\lambda_{ex} = 475$ nm, $\lambda_{em} = 592$ nm) and then compared with the standard values to obtain the doxorubicin mass loaded on the composite nano drug carrier.

According to the fluorescence test data and formula:

$$\text{Drug loading (wt\%)} = (\text{mass of drug loaded/mass of vehicle}) \times 100\%$$

$$\text{Drug loading efficiency (\%)} = (\text{mass of loaded drug/mass of injected drug}) \times 100\%$$

We studied the release performance of DOX as a carrier using the release data at different pH values.

## 2.9 Cell culture

Human melanoma cells A375 and normal human skin fibroblast GM were used for the cell experiments. The cells were incubated in Dulbecco's Modified Eagle's Medium (DMEM)

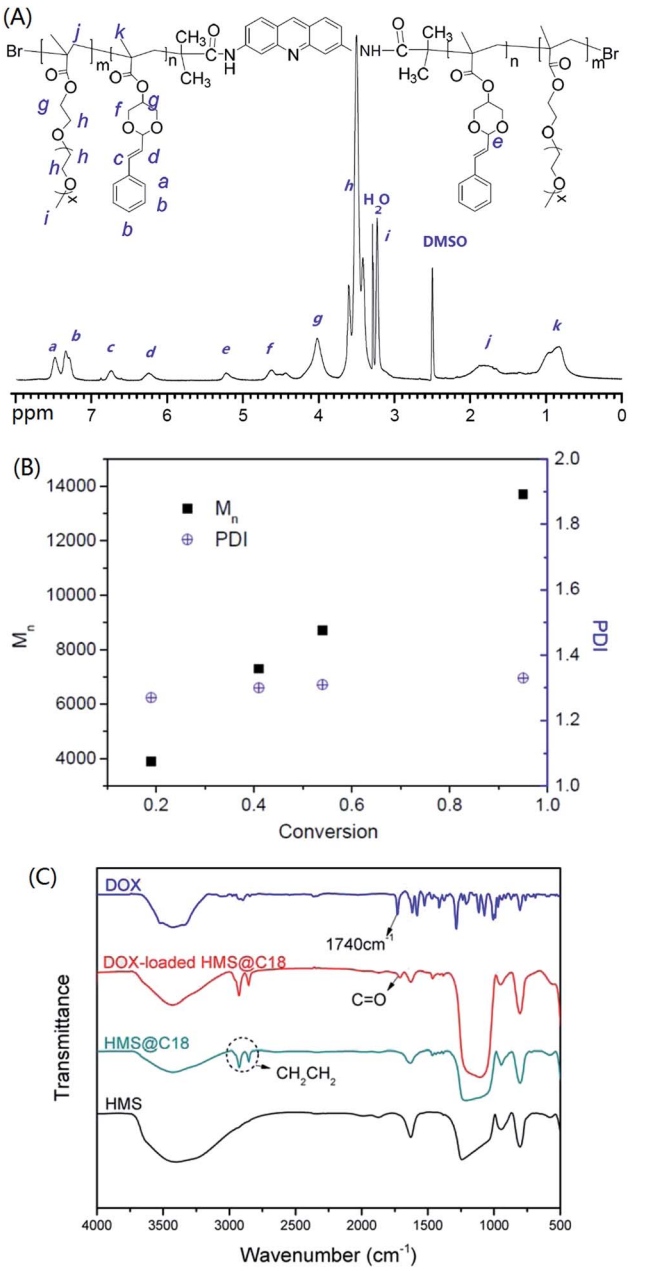


Fig. 1 $^1$H NMR spectra of PSDMA-*b*-POEGMA (DMSO-$d_6$) (A), evolution of Mn and PDI with conversion for the polymerization of PSDMA-DIA (B), and FT-IR spectra of HMS, HMS@C18 and DOX-loaded HMS@C18 (C).

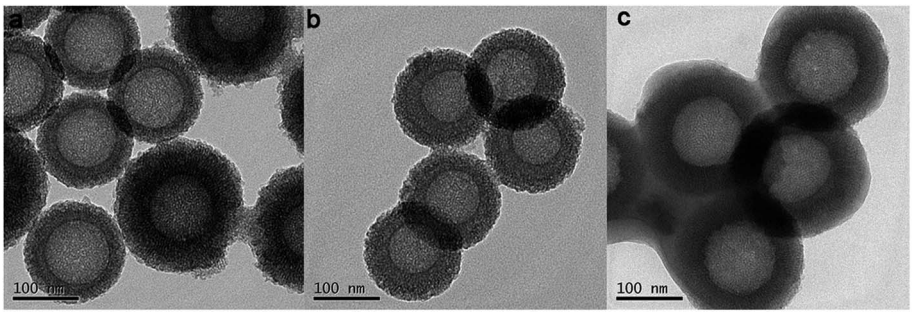


Fig. 2 TEM images of HMS (a), HMS@C18 (b) and HMS@C18@PSDMA-*b*-POEGMA (c).

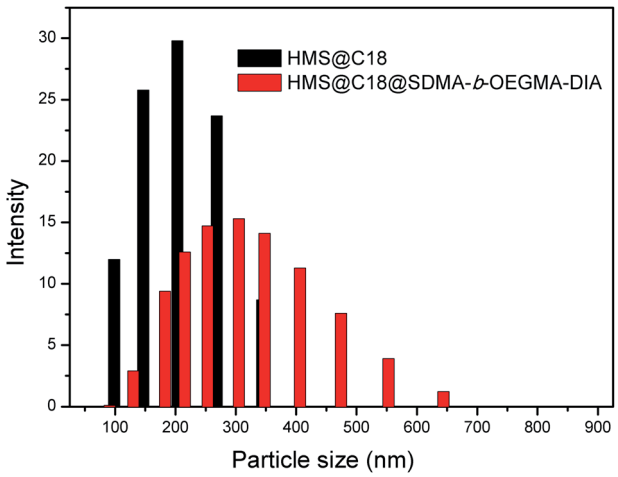


Fig. 3 DLS images of HMS@C18 and HMS@C18@PSDMA-*b*-POEGMA.

containing 10% calf serum, 50 units of penicillin and streptomycin per milliliter maintained at 37 °C and 5% carbon dioxide.

### 2.10 *In vitro* toxicity test

The cytotoxicity of the HMS@C18@PSDMA-*b*-POEGMA nanoparticles was evaluated using the 3-[4,5-dimethylthiazol-2-yl]-2,5 diphenyl tetrazolium bromide (MTT) method. The specific experimental conditions used were normal human skin fibroblasts GM in 96-well plates, wherein the number of cells in each well plate was about $2 \times 10^4$, after 24 h of incubation, the medium was replaced with a medium containing different concentrations of HMS@C18@PSDMA-*b*-POEGMA nanoparticles (0, 62.5, 125, 250, and 500 μg $mL^{-1}$, respectively). The cells were incubated for an additional 72 h, after which the medium was replaced with 100 μL of fresh DMEM and 10 μL of MTT solution (5 mg $mL^{-1}$) was added. The culture was continued for 4 h and the resulting crystals were dissolved in 100 μL DMSO. The optical density of the samples was determined at 570 nm using a BioTek microdisk meter. The results of culturing the cells alone in DMEM with phosphate buffered saline (PBS) instead of the nanoparticles were recorded as 100% survival as a standard.

The cytotoxicity tests of DOX@HMS@C18@PSDMA-*b*-POEGMA (theoretical drug loading of 5%), and the HMS nanoparticles were conducted using the same process.

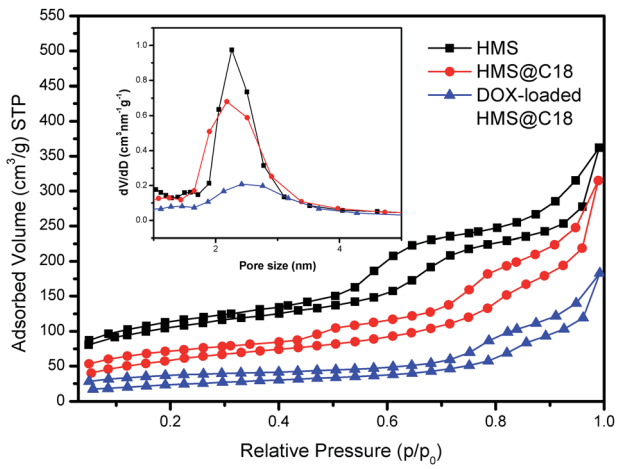


Fig. 4 $N_2$ adsorption isotherm and the corresponding pore size distribution inset of HMS, HMS@C18 and the DOX-loaded HMS@C18.

### 2.11 Uptake of simulated drugs by the cells

Human melanoma cells A375, normal human skin fibroblasts GM were inoculated in 96-well plates ($1.3 \times 10^4$ cells per well) and incubated overnight in a 37 °C incubator. The prepared drug carriers loaded with drugs were prepared in a solution with a concentration of 2 mg $mL^{-1}$ in DMEM medium, and the cells were placed in the solution for culturing for a period of time. The medium was removed, the carriers were washed with fresh culture solution three times, and then the uptake and release characteristics were observed using a live cell workstation.

Table 2 Drug loading content and drug loading efficiency for DOX with nanocomposites

| Theoretical drug loading content (wt%) | Drug loading content[a] (wt%) | Drug loading efficiency (%) |
|---|---|---|
| 5 | 4.2 | 85.8 |
| 10 | 8.0 | 77.7 |
| 50 | 36.7 | 70.4 |

[a] Drug loading content for DOX was determined by fluorescence measurements, respectively.

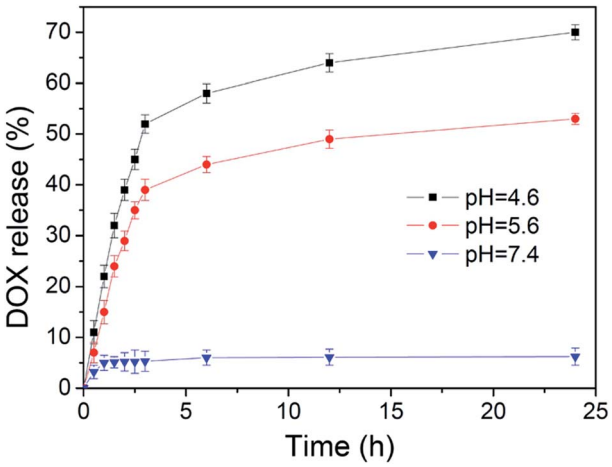


Fig. 5 The release of DOX *in vitro* from DOX-loaded HMS@C18@PSDMA-*b*-POEGMA.

# 3 Results and discussion

## 3.1 Polymerization using DIA as the initiator

The polymers PSDMA-DIA were prepared *via* ATRP using the initiator DIA. As shown in Fig. 1B, the number-average molecular weights ($M_n$) increase linearly with conversion, and the polydispersity is relatively narrow ($M_w/M_n$ = 1.27–1.33). This proved that the polymerization initiated by DIA *via* ATRP is well-controlled. The $^1$H NMR spectra of PSDMA-*b*-POEGMA (Fig. 1A) confirmed the expected structure.

## 3.2 Characterization of the nanocomposites

The infrared spectroscopy (IR) spectra of HMS@C18 and DOX-loaded HMS@C18 are shown in Fig. 1C. The peak observed for the Si–OH bond (950 cm$^{-1}$) shows that a large number of Si–OH functional groups exist on the surface of HMS, which is conducive to the modification of long alkyl chains. A strong C–$H_x$ (2850 and 2920 cm$^{-1}$) absorption peak can then be seen in the HMS@C18 diagram, indicating that the long alkyl chain was successfully attached to the surface of the silicon sphere. In DOX-loaded HMS@C18, a new absorption peak appeared at 1740 cm$^{-1}$, confirming the successful loading of DOX inside the silicon spheres.

The morphology of the HMS surface modified with C18 was almost unchanged (see Fig. 2). The hollow core was about 100 nm, and the outer layer was about 30 nm. The HMS@C18@PSDMA-*b*-POEGMA obtained after polymer coating can be easily dispersed in water, and the particle size was about 200 nm. The mesoporous layer became hazy and the wall thickness increased by about 20 nm (Fig. 2c), indicating that the polymer film on the surface layer could cover the channels of

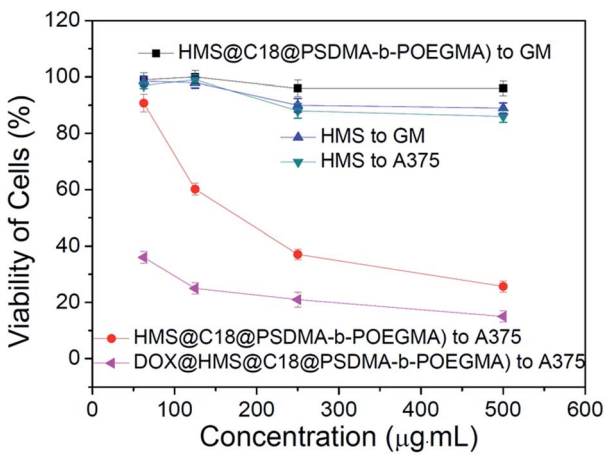


Fig. 6 Toxicity of HMS, HMS@C18@PSDMA-*b*-POEGMA and DOX@HMS@C18@PSDMA-*b*-POEGMA at different concentrations.

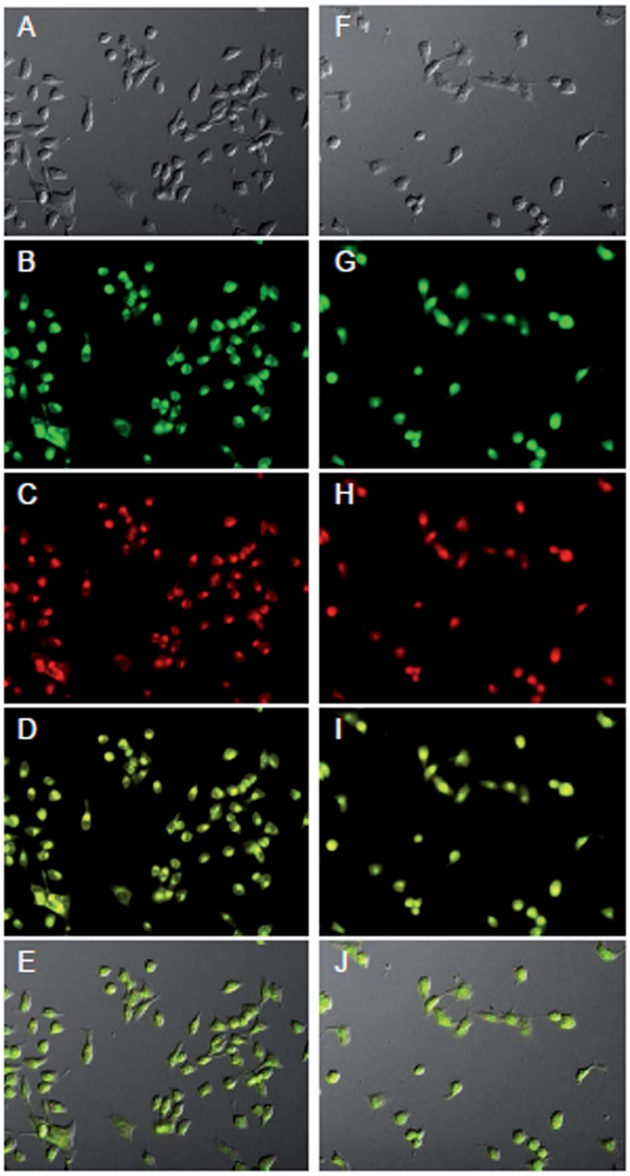


Fig. 7 Live cell imaging micrographs of A375 (A–E) and GM cells (F–J) treated with Nile Red-loaded HMS@C18@PSDMA-*b*-POEGMA nanoparticles for 30 min, including images in differential interference contrast (DIC) (A, F), in the green fluorescence channel for fluorescein (FITC) (B, G), in the red fluorescence channel for tetramethylrhodamine (TRITC) (C, H), overlaid by red and green channels (D, I), and overlaid by A and D (E), F and I (J).

the silicon spheres. The DLS results are shown in Fig. 3 and are basically consistent with the TEM results.

To further verify the hollow mesoporous structure of HMS@C18, we tested its specific surface area and pore size using nitrogen adsorption (Fig. 4). It could be seen that the specific surface area of HMS grafted with hydrophobic long-chain C18 was not significantly changed. Although the pore size was slightly reduced, $N_2$ could be smoothly adsorbed and desorbed from the pores, indicating that the pore channels of the silicon spheres were not blocked after grafting with C18, which did not affect the drug loading. The specific surface area of HMS@C18 was significantly decreased after drug loading, and the nitrogen adsorption capacity of the silicon spheres was significantly reduced after drug loading, indicating that the hollow mesoporous HMS was successfully loaded with drug molecules.

### 3.3 Drug loading and pH-sensitive release of composite nano-drug carriers

Doxorubicin is one of the most commonly used anticancer drugs, and we selected it as an anticancer drug model to test the drug loading capacity and controlled release capacity of the nanocomposite system HMS@C18@PSDMA-*b*-POEGMA. The experiments proved that the vehicle had a high drug loading efficiency under different theoretical drug loading rates (5%, 10% and 50%) (Table 2). Owing to the existence of the hollow core and the mesoporous pore channel structure, the carrier has a higher drug loading capacity which is much higher than that of common micelles and mesoporous silicon dioxide nanoparticles.

We selected samples with a theoretical drug loading of 5% as the research object to study the DOX release performance of the HMS@C18@PSDMA-*b*-POEGMA nanocomposites system (Fig. 5). To investigate the controlled release properties of pH-sensitive composite nanocarrier (DOX@HMS@C18@PSDMA-*b*-POEGMA), the prepared nanoparticles were dispersed in three buffer solutions at different pH values (7.4, 5.6, and 4.6) at 37 °C. As expected, only a very small amount (less than 10%) of the drug was released from the inside of the spheres in neutral medium (pH = 7.4) even after 24 h. However, in a weakly acidic environment (pH = 5.6, 4.6), the polymer blocking the pore

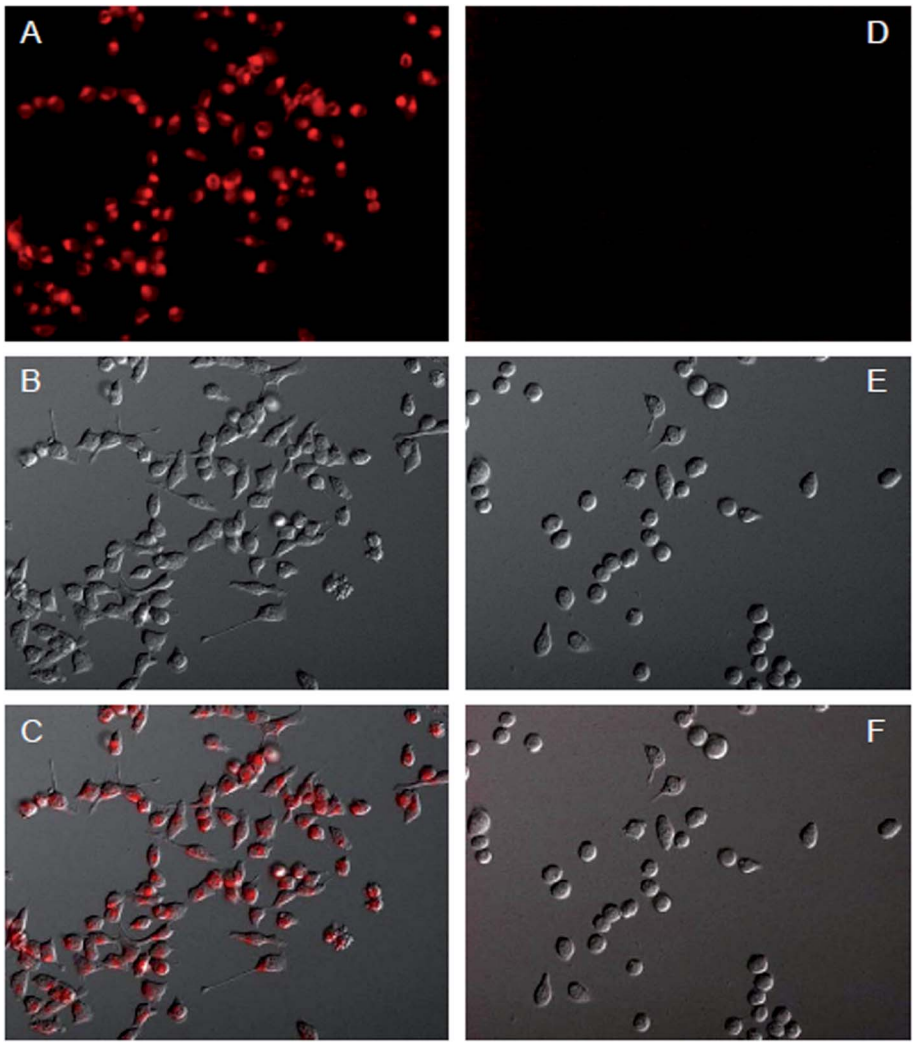


Fig. 8 Live cell imaging micrographs of A375 cells treated with Nile Red-loaded HMS@C18@PSDMA-*b*-POEGMA nanoparticles for 30 min (A–C) and 12 h (D–F), including images in the red fluorescence channel for TRITC (A, D), in DIC (B, E), and overlaid by A and B (C), D and E (F).

channels of the silicon balls is hydrolyzed, the pore channels are opened, causing the drugs in the silicon balls to be quickly released, as shown in Fig. 5. At pH values of 4.6 and 5.6, release efficiencies of 67% and 53% were achieved after 24 h, respectively. This result indicates that the nanocomposite system is expected to achieve the requirement that carriers of anticancer drugs hardly release drugs in normal tissue environments (when the pH value is neutral) and rapidly release drugs in the weakly acidic environment characteristic of tumor tissues.

### 3.4 Cytotoxicity of the composite nano-drug carriers

Different concentrations of HMS and HMS@C18@PSDMA-*b*-POEGMA were added to human melanoma cells A375 and normal human skin fibroblasts GM cultured *in vitro*. After 72 h of observation (Fig. 6) HMS is observed to be almost completely non-toxic to normal cells GM and tumor cells A375, while HMS@C18@PSDMA-*b*-POEGMA is much more toxic to the tumor cells, A375, than to normal cells, GM. Based on previously reported work, it is reasonable to speculate that the nanocomposite drug carrier selectively inhibits the growth of tumor cells owing to the small molecules of cinnamaldehyde released in the weakly acidic environment inside tumor cells. Compared with HMS@C18@PSDMA-*b*-POEGMA without DOX, DOX@HMS@C18@PSDMA-*b*-POEGMA (theoretical drug loading is 5%) is more toxic to A375. The toxicity is proposed to originate from the small molecule drug DOX and the small molecules of cinnamaldehyde released after hydrolysis.

### 3.5 Release of drug-loaded HMS@C18@PSDMA-*b*-POEGMA in cultured cells *in vitro*

To investigate the ability of HMS@C18@PSDMA-*b*-POEGMA as a drug carrier to load drugs into cells and control their release in cells, Nile red was selected as a simulated drug and used as a fluorescence probe.[24] A live cell workstation was used to observe the encapsulation and release of HMS@C18@PSDMA-*b*-POEGMA into cells. We added Nile red-loaded HMS@C18@PSDMA-*b*-POEGMA nanocomposites to the culture media of human melanoma cell A375 and human

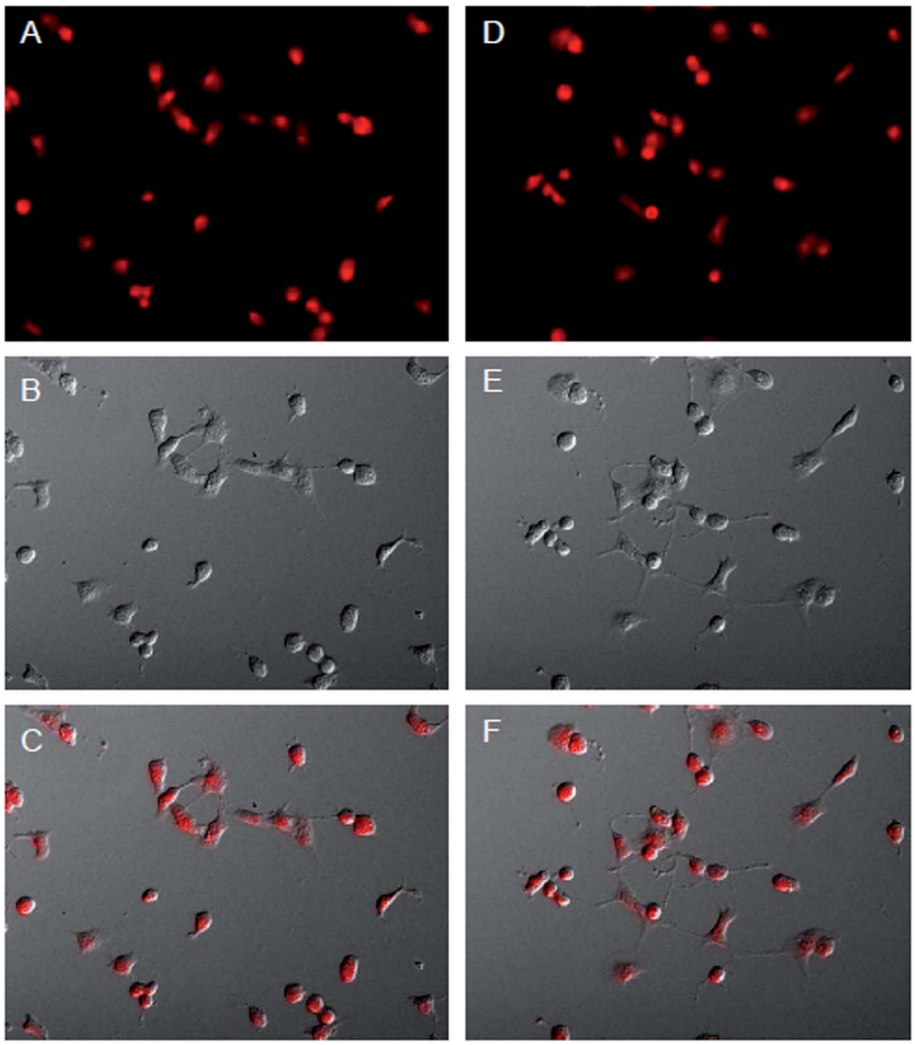


Fig. 9 Live cell imaging micrographs of GM cells treated with Nile Red-loaded HMS@C18@PSDMA-*b*-POEGMA nanoparticles for 30 min (A–C) and 12 h (D–F), including images in the red fluorescence channel for TRITC (A, D), in DIC (B, E), and overlaid by A and B (C), D and E (F).

normal fibroblast cell GM, respectively. As shown in Fig. 7, Nile red-loaded HMS@C18@PSDMA-*b*-POEGMA nanoparticles were introduced into A375 and GM cells, respectively, after further incubation for 30 min. Fig. 7A and F show cell photos under DIC, and Fig. 7B, C, G and H show fluorescence photos under different excitation wavelengths, from which we can see the green fluorescence of the HMS@C18@PSDMA-*b*-POEGMA carrier itself and the red fluorescence of the drug-loaded nanoparticles. Not only are the luminescent sites completely coincident (see Fig. 7D and I), but the overlaid yellow fluorescence is also completely consistent with the cell location (Fig. 7E and J), indicating that Nile red is successfully loaded into the inner cavity of the HMS@C18@PSDMA-*b*-POEGMA nanoparticles and can be rapidly taken up by cells A375 and GM.

However, after continuous culture for 12 h, the fluorescence intensity of Nile red in the A375 cells was significantly weakened, indicating that the polymer PSDMA-*b*-POEGMA loaded with Nile red on the surface of the HMS@C18@PSDMA-*b*-POEGMA nanoparticles was hydrolyzed in the weakly acidic environment of the tumor cell endosome/lysosome, and the channels in the originally blocked silicon spheres were opened to release Nile red. In addition, significant changes in the activity of the A375 cells and the cell morphology could be observed (Fig. 8), showing that the small molecules of cinnamic aldehyde released by nanoparticle water interpretation inhibited the melanoma cell A375. On the other hand, when the Nile red-loaded HMS@C18@PSDMA-*b*-POEGMA nanoparticle solution was also added for continuous culture for 12 h, the cell morphology and fluorescence intensity of the GM cells showed no significant changes compared with those after 30 min of culture (Fig. 9). In summary, we believe that Nile red-loaded HMS@C18@PSDMA-*b*-POEGMA nanoparticles can rapidly enter cells, but only rapidly release drugs and small molecules of cinnamic aldehyde in the weakly acidic environment of tumor cells.

## 4 Summary

In this study, the pH-sensitive amphiphilic block copolymer PSDMA-*b*-POEGMA with a green fluorescent group was designed and synthesized. The HMS was coated by physical action, and the obtained nanocomposite could be used for the controlled release of drugs and fluorescence imaging. The pH sensitive polymer was prepared using an ATRP method, and an amphiphilic block polymer PSDMA-*b*-POEGMA was formed by initiating a pH sensitive monomer (SDMA) and a hydrophilic monomer (OEGMA) using a fluorescence initiator (DIA). Then, they self-assembled with hollow mesoporous silica (HMS@C18) with long alkyl chains to form pH-sensitive core–shell nanoparticles (HMS@C18@PSDMA-*b*-POEGMA). The HMS@C18@PSDMA-*b*-POEGMA nanoparticles have a high drug loading capacity and pH-controlled release effect. The obtained nanocarrier showed a high drug loading content owing to the hollow core and mesopores of the HMS. As cell imaging is possible owing to the green fluorescence, after the loaded drug enters the human melanoma cell A375, it can be observed that the antitumor drug and the cinnamic aldehyde small molecule, which has a specific inhibition effect on the melanoma cell, are released in the weakly acidic environment within the cell body. Thus, the pH sensitive nanoparticles selectively inhibit the growth of human melanoma cells A375 relative to human normal fibroblasts GM.

## Conflicts of interest

There are no conflicts to declare.

## Acknowledgements

We gratefully acknowledge the Qing-Lan Project of Jiangsu Province (2018) and the Natural Science Foundation of the Jiangsu Higher Education Institutions of China (No. 18KJD610001).

## References

1 J. Lu, N. Li, Q. Xu, J. Ge, J. Lu and X. Xia, Acetals Moiety Contained pH-sensitive Amphiphilic Copolymer Selfassembly Used for Drug Carrier, *Polymers*, 2010, **51**, 1709–1715.
2 J. S. Wang and K. Matyjaszewski, Controlled/"living" radical polymerization, atom transfer radical polymerization in the presence of transition-metal complexes, *J. Am. Chem. Soc.*, 1995, **117**, 5614–5615.
3 J. S. Wang and K. Matyjaszewski, Controlled/"living" radical polymerization. Halogen atom transfer radical polymerization promoted by a Cu (I)/Cu (II) redox process, *Macromolecules*, 1995, **28**, 7901–7910.
4 C. N. Yan, Q. Liu, L. Xu, L. P. Bai, L. P. Wang and G. Li, Photoinduced Metal-Free Surface Initiated ATRP from Hollow Spheres Surface, *Polymers*, 2019, **11**, 599–611.
5 A. Diacon, E. Rusen, A. Mocanu and L. C. Nistor, Supported $Cu^0$ nanoparticles catalyst for controlled radical polymerization reaction and block-copolymer synthesis, *Sci. Rep.*, 2017, **7**, 10345–10354.
6 Y. Wang, M. Nguyen and A. J. Gildersleeve, Macromolecular Engineering by Applying Concurrent Reactions with ATRP, *Polymers*, 2020, **12**, 1706–1721.
7 M. Ouchi, T. Terashima and M. Sawamoto, Transition Metal-Catalyzed Living Radical Polymerization: Toward Perfection in Catalysis and Precision Polymer Synthesis, *Chem. Rev.*, 2009, **109**, 4963–5050.
8 S. Li, H. S. Chung, A. Simakova, Z. Wang, S. Park, L. Fu, D. Cohen-Karni, S. Averick and K. Matyjaszewski, Biocompatible Polymeric Analogues of DMSO Prepared by Atom Transfer Radical Polymerization, *Biomacromolecules*, 2017, **18**, 475–482.
9 S. A. Bencherif, D. J. Siegwart, A. Srinivasan, F. Horkay, J. O. Hollinger, N. R. Washburn and K. Matyjaszewski, Nanostructured hybrid hydrogels prepared by a combination of atom transfer radical polymerization and free radical polymerization, *Biomaterials*, 2009, **30**, 5270–5278.

10 H. Hyun, J. Park, K. Willis, J. E. Park, L. T. Lyle, W. Lee and Y. Yeo, Surface modification of polymer nanoparticles with native albumin for enhancing drug delivery to solid tumors, *Biomaterials*, 2018, **180**, 206–224.

11 H. Chen, D. Sulejmanovic, T. Moore, D. C. Colvin, B. Qi, O. T. Mefford, J. C. Gore, F. Alexis, S. J. Hwu and J. N. Anker, Iron-Loaded Magnetic Nanocapsules for pH-Triggered Drug Release and MRI Imaging, *Chem. Mater.*, 2014, **26**, 2105–2112.

12 F. Chen, H. Hong, S. Shi, S. Goel, H. F. Valdovinos, R. Hernandez, C. P. Theuer, T. E. Barnhart and W. Cai, Engineering of hollow mesoporous silica nanoparticles for remarkably enhanced tumor active targeting efficacy, *Sci. Rep.*, 2014, **4**, 5080–5089.

13 L. Pang, Y. Pei, G. Uzunalli, H. Hyun, L. T. Lyle and Y. Yeo, Surface Modification of Polymeric Nanoparticles with M2pep Peptide for Drug Delivery to Tumor-Associated Macrophages, *Pharm. Res.*, 2019, **36**, 65–87.

14 S. P. Hadipour Moghaddam, M. Yazdimamaghani and H. Ghandehari, Glutathione-sensitive hollow mesoporous silica nanoparticles for controlled drug delivery, *J. Control. Release*, 2018, **282**, 62–75.

15 J. Shen, R. Wang, Q. Wang, M. Zhang, C. Liu, Z. Tao and G. Su, The improved anticancer effects of Bortezomib-loaded hollow mesoporous silica nanospheres on lymphoma development, *Aging*, 2020, **13**, 411–423.

16 S. B. Hartono, N. Truong Phuoc, M. Yu, Z. Jia, M. J. Monteiro, S. Qiao and C. Yu, Functionalized large pore mesoporous silica nanoparticles for gene delivery featuring controlled release and co-delivery, *J. Mater. Chem. B*, 2014, **2**, 718–726.

17 X. Mei, D. Chen, N. Li, Q. Xu, J. Ge, H. Li and J. Lu, Hollow mesoporous silica nanoparticles conjugated with pH-sensitive amphiphilic diblock polymer for controlled drug release, *Microporous Mesoporous Mater.*, 2012, **152**, 16–24.

18 Q. Zhou, P. Gu, Y. Zhang, N. Li, Q. Xu, Y. Zhang and J. Lu, Preparation of Fluorescent Polystyrene via ATRP with Dimethylamino Chalcones as Initiator, *Chin. J. Chem.*, 2014, **32**, 573–578.

19 D. Chen, Z. Luo, N. Li, J. Y. Lee, J. Xie and J. Lu, Amphiphilic Polymeric Nanocarriers with Luminescent Gold Nanoclusters for Concurrent Bioimaging and Controlled Drug Release, *Adv. Funct. Mater.*, 2013, **23**, 4324–4331.

20 M. N. Vu, H. G. Kelly, A. K. Wheatley, P. Scott, E. H. Pilkington, N. A. Veldhuis, T. P. Davis, S. J. Kent and N. P. Truong, Cellular Interactions of Liposomes and PISA Nanoparticles during Human Blood Flow in a Microvascular Network, *Small*, 2020, **16**(33), 2002861.

21 D. Chen, Q. Xu, X. Xia, J. Ge, J. Lu and N. Li, A novel pH-sensitive polymeric fluorescent probe: synthesis, characterization and optical properties, *Mater. Chem. Phys.*, 2010, **120**, 614–618.

22 H. Hibbert and M. S. Whelen, Studies on reactions relating to carbohydrates and polysaccharides. xxii. The isomeric cinnamylidene glycerols, *J. Am. Chem. Soc.*, 1929, **51**, 620–625.

23 H. Yan, Z. Zhang, X. Jia and J. Song, D-α-Tocopheryl polyethylene glycol succinate/solutol HS 15 mixed micelles for the delivery of baohuoside I against non-small-cell lung cancer: optimization and in vitro, in vivo evaluation, *Int. J. Nanomedicine*, 2016, **11**, 4563–4571.

24 N. P. Truong, J. F. Quinn, M. V. Dussert, N. B. T. Sousa, M. R. Whittaker and T. P. Davis, Reproducible Access to Tunable Morphologies via the Self-Assembly of an Amphiphilic Diblock Copolymer in Water, *ACS Macro Lett.*, 2015, **4**, 381–386.